ETH_zürich_

15N transverse relaxation measurements for the characterization of µs–ms dynamics are deteriorated by the deuterium isotope effect on 15N resulting from solvent exchange

^{15}N Transverse Relaxation Measurements for the Characterization of μs-ms Dynamics are Deteriorated by the Deuterium Isotope Effect on ^{15}N resulting from Solvent Exchange

Pratibha Kumari[1], Lukas Frey[1], Alexander Sobol[1], Nils-Alexander Lakomek[1]*, Roland Riek[1]*

^{1}ETH Zürich, Department of Chemistry and Applied Biosciences, Laboratory of Physical Chemistry, Vladimir-Prelog-Weg 2, 8093 Zürich, Switzerland

*correspondence:

Dr. Nils-Alexander Lakomek

e-mail: nils-alexander.lakomek@phys.chem.ethz.ch, phone : +41 44 632 4371,

 Orcid.org/0000-0002-4285-6339

Prof. Dr. Roland Riek

e-mail: roland.riek@phys.chem.ethz.ch, phone : + 41 44 633 4259

Dedication: This manuscript is dedicated to Alexander Sobol.

Abstract. ^{15}N R_2 relaxation measurements are key for the elucidation of the dynamics of both folded and intrinsically disordered proteins (IDPs). Here we show, on the example of the intrinsically disordered protein α-synuclein and the folded domain PDZ2, that at physiological pH and near physiological temperatures amide – water exchange can severely skew Hahn-echo based ^{15}N R_2 relaxation measurements as well as low frequency data points in CPMG relaxation dispersion experiments. The nature thereof is the solvent exchange with deuterium in the sample buffer, which modulates the ^{15}N chemical shift tensor via the deuterium isotope effect, adding to the apparent relaxation decay which leads to systematic errors in the relaxation data. This results in an artificial increase of the measured apparent ^{15}N R_2 rate constants – which should not be mistaken with protein inherent chemical exchange contributions, R_{ex}, to ^{15}N R_2. For measurements of ^{15}N R_2 rate constants of IDPs and folded proteins at physiological temperatures and pH, we recommend therefore the use of a very low D_2O molar fraction in the sample buffer, as low as 1%, or the use of an external D_2O reference along with a modified ^{15}N R_2 Hahn-echo based experiment. This combination allows for the measurement of R_{ex} contributions to ^{15}N R_2 originating from conformational exchange in a time window from μs to ms.

Introduction

Proteins are inherently dynamic systems with motions that cover a several orders of magnitude wide time scale from femtosecond to more than seconds[1,2]. Such dynamics may be local, concerted, correlated or of anti-correlated nature [3-7]. Nuclear magnetic resonance spectroscopy (NMR) is one of the major methods to study protein dynamics. A plethora of NMR experiments have been and are further being developed to elucidate protein motions [2,6,8-14]. One of the standard experiments are ^{15}N R_1, R_2 relaxation measurements and the ^{15}N NOE experiment for the detection of the rotational correlation time of the molecule under study as well as local fast dynamics at a residue-specific resolution (i.e. for each ^{15}N-^{1}H

moiety along the amino acid sequence) [15,16]. These measurements have been complemented with more sophisticated experiments and analyses to obtain also intermediate and slow time scale information from µs up to ms. This includes the ^{15}N CPMG- or ^{15}N R$_{1\rho}$ based relaxation dispersion experiments [17,18], CEST or DEST measurements [9,12] and alternatively ^{13}C methyl relaxation measurements covering protein side-chain dynamics [19,20]. Towards a more comprehensive picture of dynamics, residual-dipolar couplings[11,21,22], cross-correlated relaxation [4,7,23], paramagnetic relaxation enhancement (PRE) [24-26] and eNOE-based [6,27] data have been acquired and can be used in combination with molecular dynamics simulation [28,29] or ensemble averaging [5,11,27,30,31] and chemical-shift based structural ensemble prediction [32-34].

For the investigation of µs-ms dynamics, ^{15}N R$_2$ measurements are among the most frequently used experiments. The ^{15}N R$_2$ rate constant, which describes the decay of ^{15}N transverse magnetization as measured e.g. in a Hahn-echo experiment, has an exchange contribution, R$_{ex}$, due to conformational and chemical exchange that modulates the ^{15}N chemical shift tensor [35,36] that adds to the R$_{2,0}$ auto-relaxation rate constant: R$_2$ = R$_{2,0}$ + R$_{ex}$.

It is probably surprising that the presented work identifies a systematic error in several ^{15}N R$_2$ relaxation measurements for the characterization of µs-ms dynamics that deteriorates the dynamics analysis of proteins and in particular intrinsically disordered proteins (IDP) and protein loops when measured under physiological conditions (i.e. pH ~7.4 and at a temperature of ~37 °C). The identified culprit is the fast exchange of the amide protons with water and simultaneously with the internal reference substance, D$_2$O, resulting in an exchange contribution induced by the deuterium-induced isotope shift of ^{15}N, that becomes particularly acute at physiological pH and temperatures. We exemplify this effect using Hahn-echo based ^{15}N R$_2$ measurements that do not suppress exchange contributions and CPMG relaxation dispersion measurements on α-synuclein, which is an IDP associated to Parkinson's disease, as well as the PDZ2 domain of human phosphatase and provide a straightforward solution (i.e. the use of a very low D$_2$O molar fraction, as low as 1%, or, alternatively, the use of an external D$_2$O lock and the appropriate pulse sequence).

Material and Methods

Protein expression and purification

Acetylated α-synuclein was expressed using co-expression of the N-terminal acetyltransferase B (NatB) complex and the α-synuclein plasmid (pRK172), as described earlier [37]. Expression and purification were performed as described earlier [38], with some modification. Briefly, after transformation, colonies containing both plasmids (NatB and pRK172) were grown at 37 °C in 10 ml Lysogeny Broth (LB) medium overnight and were then transferred into 1 L of LB media. After reaching an OD_{600} of around 0.5, cells were harvested by centrifugation and resuspended into 1 L M9 minimal media containing $^{15}NH_4Cl$ and grown till an OD_{600} of 1.0 was reached. Protein expression was carried out overnight at 37 °C, after induction with 1 mM IPTG. Cells were harvested by centrifugation and α-synuclein, present in the periplasm, were purified using ion exchange chromatography and hydrophobic interaction chromatography as described earlier [39].

The PDZ2 domain from human phosphatase (hPTP1E) was encoded into a pET21 expression system with a T7 promoter and Histidine tag. Expression and purification were performed as described earlier [40], with some modifications. After transformation, a single colony was inoculated overnight in 10 ml LB medium at 37 °C and then transferred into 1 L M9 minimal media containing $^{15}NH_4Cl$ and grown till an OD_{600} of 0.5 was reached. Protein expression was induced by adding 1 mM IPTG and cells were harvested by centrifugation after 5 h. A Ni-affinity column (HisTrap FF) was used for purification of protein and the histidine-tag was cleaved with Human Rhinovirus 3C (HRV 3C) followed by another Ni-affinity column purification step.

NMR Measurements

NMR spectra were recorded with 500 μM of ^{15}N-labeled acetylated α-synuclein dissolved in 20 mM Tris (pH 7.4) and 100 mM NaCl, unless indicated differently. Spectra of ^{15}N-labeled PDZ domain, dissolved in 50 mM sodium phosphate buffer (pH 8.0) and 150 mM NaCl, were recorded at an experimental temperature of 303 K. ^{15}N TROSY- R_2^{β} rate constants were measured by applying the NMR experiment described earlier [41]. ^{15}N R_2 experiments, applying proton decoupling during the

relaxation delay period [36], were recorded using the pulse sequence described in Fig. 1. For proton decoupling, waltz64 with an RF amplitude of 2.5 kHz was applied. ^{15}N $R_{1\rho}$ rate constants were recorded using the NMR experiment described in [42]. CPMG-based ^{15}N R_2 rate constants were determined using a proton-decoupled CPMG experiment, similar to the one described by Yuwen and Skrynnikov[43], however using waltz64 with an RF amplitude of 2.5 kHz for proton decoupling rather than DIPSI2. ^{15}N R_2 rate constants were measured for the two CPMG frequencies, 20 Hz and 100 Hz. All NMR experiments were performed on a Bruker 600 MHz Avance III HD spectrometer equipped with cryogenic probe. Spectral dimensions were $\Omega(^1H)$ x $\Omega(^{15}N)$ = 14.014 ppm x 35 ppm. 512 complex points were recorded in the direct dimension (^1H) and 80 complex points in the indirect dimension (^{15}N), resulting in an acquisition time of 60.08 ms in the direct and 37.5 ms in the indirect dimension, respectively. The ^1H carrier was set to 4.7 ppm and the ^{15}N carrier to 118 ppm, respectively. The magnetization decay was recorded using four different relaxation decay periods, in an inter-leaved manner [42]. For α-synuclein, R_2 relaxation delays were set to 0 ms, 200 ms, 100 ms, and 50 ms and for the ^{15}N $R_{1\rho}$ experiments, delays were set to 1 ms, 120 ms, 60 ms, and 20 ms, respectively. The spin-lock RF field strength in the ^{5}N $R_{1\rho}$ measurement was set to 2 kHz. For experiments using the ^{15}N TROSY-R_2^{β} sequence decay periods differed slightly; at pH 7.4 and at a temperature of 303 K or 283 K delays were 0, 100, 50, and 20 ms. Spectral intensities for the different decay periods were recorded in an inter-leaved manner, 16 scans were recorded for each decay period. The total experimental time was 4.75 h. For the PDZ domain, relaxation delays were set to 0 ms, 50 ms, 30 ms, and 10 ms. For the CPMG experiments, a fixed relaxation delay of 200 ms was used. Relaxation data where recorded for two different CPMG frequencies, 100 Hz and 20 Hz by adjusting the number of 180˚(N) pulses and the inter-pulse delay accordingly.

The software Sparky 3.115 (T. D. Goddard and D. G. Kneller, SPARKY 3, University of California, San Francisco, USA) and Bruker Topspin 3.5pl7 (Bruker, Inc., Billerica, MA, USA) were used for analyzing the spectra and extracting the rate constants.

NMR spectra recorded on samples containing D_2O in the sample buffer were measured using a regular Shigemi tube (Sigma-Aldrich, Merck KGaA, Darmstadt, Germany). For samples without D_2O in the

sample buffer, D_2O was added as an external reference using a Wilmad coaxial insert (stem length 50 mm, 2 mm diameter) and the sample was kept in a thin wall 5 mm NMR tube (Wilmad NMR tubes, 5 mm diam., precision, Sigma-Aldrich, Merck KGaA, Darmstadt, Germany). The coaxial insert containing D_2O was inserted into the 5 mm thin-wall NMR tube containing the sample.

Simulation of CPMG relaxation dispersion curves

CPMG relaxation dispersion curves were calculated using the formula:

$$R_{ex} = p_H p_D \Delta\omega^2 k_{ex} / \left[k_{ex}^2 + \left(p_H^2 \Delta\omega^4 + 144/\tau_{CP} \right)^{1/2} \right] \tag{1}$$

as described in [44,45], with the basic CPMG element $\tau_{CP}/2 - 180° - \tau_{CP}/2$. The inter-pulse delay τ_{CP} relates to the CPMG frequency ν_{CPMG} via $\nu_{CPMG} = 1/(2\tau_{CP})$. The chemical shift difference induced by the deuterium isotope effect is $\Delta\delta(N) = 687 \pm 35$ ppb [46] which amounts to ca. $\Delta\omega = 250$ rad s^{-1} and $\Delta\omega/2\pi = 40$ Hz at a magnetic field strength of 14.1 T (corresponding to a proton Larmor frequency of 600 MHz) and k_{ex} is equal to the assumed amide solvent exchange rate constant (see Results section for derivation); p_D is the population of deuterium in the sample buffer (e.g. 0.1 for 10% D_2O) and p_H the population of H_2O in the sample buffer.

Results

Pulse sequence for the measurement of ^{15}N R_2 relaxation

The average backbone amide exchange rate constant shows a strong pH dependence, with a minimum around pH 3 (10^{-1} / min at 298 K) and a ten-fold increase for each pH unit [47,48], resulting in ca. 10^2 / min at pH 6 (298 K) and roughly 10^3 / min at pH 7.4 (298 K). Indeed, for α-synuclein at 288 K, measured amide solvent exchange rates varied between 2 and 20 s^{-1} for different residues at low salt concentration (20 mM) and between 10 s^{-1} and 80 s^{-1} for high salt concentrations (300 mM)[49]. With the emphasis to measure ^{15}N relaxation of α-synuclein at physiological conditions including physiological temperature (i.e. 303 K) we have therefore selected an NMR pulse sequence that measures the transverse relaxation

of ^{15}N in-phase coherence, with proton decoupling applied during the relaxation period to alleviate the impact of exchange of the ^{15}N-^{1}H moiety with water. By that, evolution into anti-phase $N_{x/y}H_z$ coherence is minimized (Fig. 1). This is different from e.g. ^{15}N TROSY- R_2^{β} experiments using a Hahn-echo based pulse sequence element (Fig. S1) [41,50]. Because if anti-phase $N_{x/y}H_z$ coherence is present or evolves during the Hahn-echo relaxation delay in presence of amide exchange, amide exchange will lead to decorrelation of two spin-order [51]. This loss of the $N_{x/y}H_z$ coherence will lead to an artificial extra relaxation contribution to the measured ^{15}N R_2, rate constant as illustrated in Fig. S2 (this artificial extra relaxation contribution is denoted $R_{ex,amide}$ in Fig. S2).

In Fig. 1, a TROSY-based and Hahn-echo based ^{15}N R_2 experiment is shown that avoids this bias introduced by amide exchange. In details, anti-phase ^{15}N magnetization generated after the first INEPT transfer is transferred further to in-phase ^{15}N magnetization in the second step of the re-focused INEPT transfer (b). Therefore, at the beginning of the relaxation period, N_x in-phase magnetization is present. After a z-filter (c), in-phase N_x magnetization is subject to transverse ^{15}N R_2 relaxation during the Hahn-echo element. Importantly, the generation of anti-phase magnetization is minimized by ^{1}H decoupling (d). After a second z-filter (e), gradient as well as phase-cycling based echo / anti-echo encoding is achieved prior to t_1 evolution. After t_1 evolution (f), $N_{x/y}H^{\beta}$ coherence is transferred to $H_{x/y}N^{\beta}$ coherence during a TROSY-read out scheme, opening this pulse sequence also for large systems [52] (g), which then evolves during acquisition. Further, ^{15}N magnetization, transferred from ^{1}H during the TROSY read-out scheme is   destroyed by a 90° pulse on ^{15}N (h) [42,53]. Note that in this experiment, ^{15}N $R_{2,0}$ auto-relaxation (plus R_{ex} contribution) and therefore the average of fast and slowly relaxing NH doublet components is measured rather than the decay of the slowly relaxing $N_{x/y}H^{\beta}$ line, which is measured in the ^{15}N TROSY-R_2^{β} experiment [41]. The relevance of selecting a ^{15}N-inphase-based pulse sequence becomes apparent when comparing the ^{15}N relaxation rate constants measured for the intrinsically disordered protein α-synuclein using the pulse sequence of Fig. 1 compared to those measured using the ^{15}N TROSY-R_2^{β} experiment [41] (see Fig. S3).
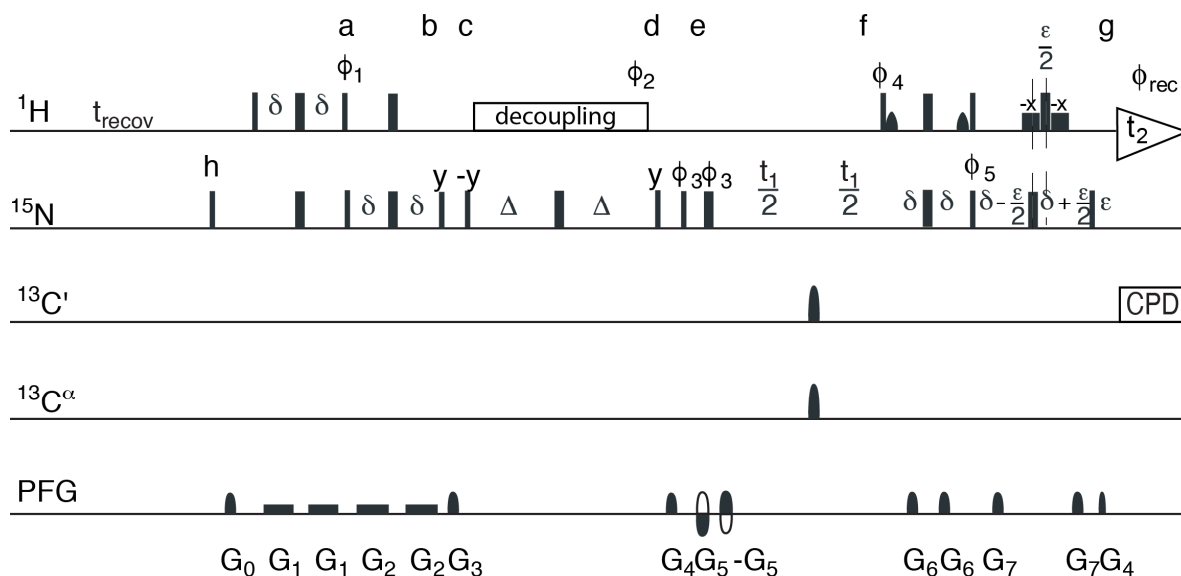
Fig. 1. **Pulse scheme for the ^{15}N R_2 relaxation (Hahn-echo) experiment**. ^{1}H magnetization is transferred to ^{15}N in-phase magnetization via a refocused INEPT transfer. After a z-filter, a Hahn echo (Δ - 180º(N) – Δ) with the variable relaxation delay Δ is performed. ^{1}H decoupling during the Hahn echo minimizes the evolution of the anti-phase term during the relaxation period. Echo/ anti-echo encoding for quadrature detection is performed prior to the t_1 evolution period. Narrow rectangles indicate hard 90° pulses and broader rectangles hard 180° pulses. The rectangular ^{1}H pulses marked –x are low power 90º pulses (1.2 ms at 600 MHz); shaped low power ^{1}H pulses (1.9 ms) correspond to the center lobe of a (sin$x$)/x function, all serving to return the water magnetization to z prior to detection [54]. For application to samples that also are enriched in ^{13}C: durations of ^{13}C pulses (all 180°) are equal to $\frac{\sqrt{3}}{2\Omega}$ (47.4 μs at 600 MHz), where Ω is the frequency difference between ^{13}C$^{\alpha}$ and ^{13}C'. Delay durations are δ = 2.65 ms and ε corresponds to the duration of the decoding gradient G_4 (60.8 μs; the slight offset ($\varepsilon/2$) relative to the ^{15}N 180º pulse enables insertion of the decoding gradient G_4, without introducing a linear phase error in the ^{1}H dimension. Gradients: G_0 (1000 μs; 21 G/cm), G_1 (2650 μs; 0.7 G/cm), G_2 (2550 μs; 1.4 G/cm), G_3 (500 μs; 42 G/cm), G_4 (1000 μs; 7 G/cm), G_5 (300 μs; -23 G/cm), G_6 (300 μs; 7 G/cm), G_7 (1000 μs; 35 G/cm) and G_8 (60.8 μs; 23 G/cm) are sine-bell shaped. Phase cycling: φ_1= 8(y), 8(-y); φ_2 = y; and φ_3 = y, x, -y, -x,-y,-x ,y ,x; φ_4 = y; φ_5 = y and φ_{rec}=y,-x,-y, x, -y, x, y, -x, -y, x, y, -x, y, -x, -y, x. Quadrature detection is implemented using the Rance-Kay echo/anti-echo scheme [55], with the polarity of gradients G_5 and –G_5 inverted, and φ_3= y, -x, -y, x, -y, -x, y, x, φ_4 = -y and φ_5 = -y for the second FID generated for each quadrature pair. The relaxation decay of ^{15}N (in-phase) coherence is sampled at different delay durations Δ in an inter-leaved manner.

^{15}N R_2 relaxation contribution by the deuterium isotope effect

Measuring ^{15}N relaxation of α-synuclein at physiological conditions (i.e. pH 7.4 and 303 K) using the pulse sequence shown in Fig. 1, we noticed a variation of extracted rate constants, depending on the

D$_2$O molar fraction in the sample buffer. This is demonstrated in Fig. 2, for which ^{15}N R$_2$ rate constants of α-synuclein were measured in 4 %, 10 %, and 50 % D$_2$O, respectively. The apparent rate constants measured are significantly elevated with increased D$_2$O, apart from C-terminal residues 110 to 140 that do not show any significant increase, due to exchange protection through hydrogen bond formation of acidic-side chains with amide groups [56].
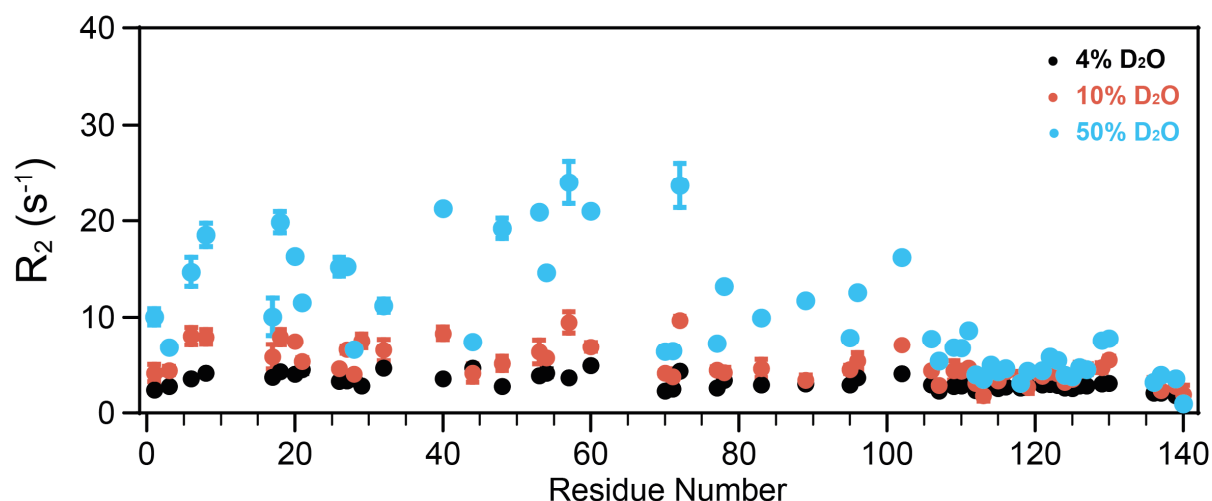

Fig. 2. **D$_2$O-dependent ^{15}N relaxation rate constants.** ^{15}N R$_2$ rate constants of ^{15}N-labeled α-synuclein, measured using the pulse sequence shown in Fig. 1 and in the presence of (A) 4% (black), 10% D$_2$O (red), or 50% D$_2$O (blue). The experimental temperature was 303 K and the pH was 7.4. The increase of the relaxation rates with increase of D$_2$O identifies D$_2$O as a culprit for ^{15}N transverse relaxation measurements.

This finding points to a R$_{ex}$ contribution because of the deuterium isotope effect that modulates the ^{15}N chemical shift tensor due to exchange between protons and deuterons in the amide group at an exchange rate constant, k$_{ex}$, which is equal to the solvent exchange rate constant[57]. This can be seen as follows: The residue-specific k$_{ex}$ is the sum of the forward and backward pseudo first order reaction rate constant, k$_{HD}$ and k$_{DH}$, respectively, where k$_{HD}$ is the product of the amide solvent exchange rate constant, k$_{NH}$, describing the exchange of amide protons with water, and the likelihood that an exchange to a deuteron takes place instead of a proton, which is equal to the population of D$_2$O in the sample buffer, p$_D$: $k_{HD} = k_{NH} \times p_D$. Vice versa, the rate constant for the backward reaction is $k_{DH} = k_{ND} \times p_H$ where p$_H$ is the

population of H_2O in the sample buffer and k_{ND} the exchange of the amide deuterium with water. It is assumed that $k_{ND} = k_{NH}$ [58]. This yields:

$$k_{ex} = k_{HD} + k_{DH} = k_{NH}(p_D + p_H) = k_{NH} \quad (2)$$

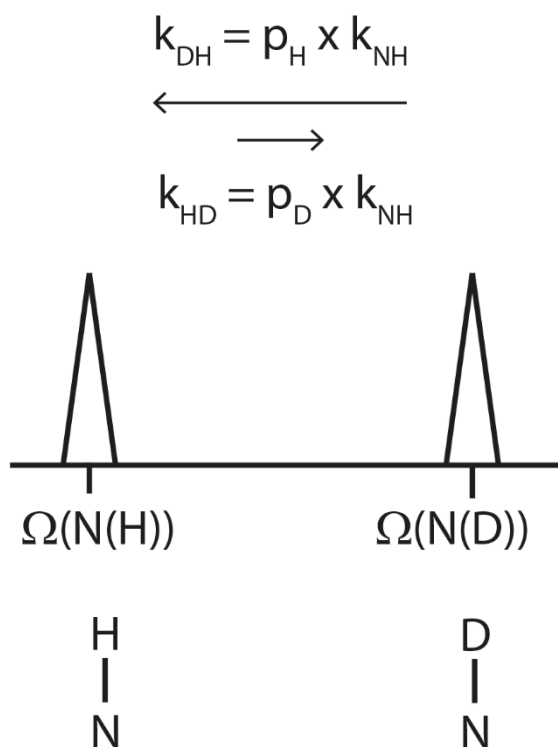Fig. 3 illustrates the described process.

Fig. 3. Chemical exchange between and amide N-H and N-D moiety changes the resonance frequency of the ^{15}N nucleus by changing the chemical shift tensor via the deuterium isotope effect. In equilibrium, the rate constant that describes the conversion from N-H to N-D is described by the solvent amide exchange rate multiplied with the population of D_2O in the sample buffer. The backward reaction from N-D to N-H is described by the solvent amide exchange rate times the population of H_2O in the sample buffer. It is thereby assumed that the exchange of the amide deuterium with water is equal to the exchange of an amide proton with water [58].

The exchange rate constant describing the modulation of the chemical shift tensor can also be obtained from a kinetic derivation as we shall see:

$$NH + D_2O \xrightarrow{k_{HD}^{(2)}} ND + HDO \qquad (3a)$$

$$ND + H_2O \xrightarrow{k_{DH}^{(2)}} NH + HDO \qquad (3b)$$
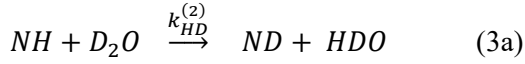
Equation (3a) ad (3b) are of pseudo first order, since both the H_2O and D_2O molar fractions are much higher than the protein molar fraction in water. Therefore, we obtain:

$$NH \xrightarrow{k_{HD}^{(2)} [D_2O]} ND \qquad (4a)$$

$$ND \xrightarrow{k_{DH}^{(2)} [H_2O]} NH \qquad (4b)$$

with the pseudo first order rate constants:

$$k_{HD} = k_{HD}^{(2)} [D_2O] = k_{HD}^{(2)} [H_2O]_0 \times p_D = k_{NH} \times p_D \text{ (5a)}$$

and

$$k_{DH} = k_{DH}^{(2)} [H_2O] = k_{DH}^{(2)} [H_2O]_0 \times p_H = k_{NH} \times p_H \quad (5b)$$

where $[H_2O]_0$ is the molar fraction of H_2O in the sample buffer in the absence of D_2O; p_D is the population of D_2O and p_H is the population of H_2O in the sample buffer, resulting in an actual molar fraction $[H_2O] = [H_2O]_0 \times p_H$ of H_2O and $[D_2O] = [H_2O]_0 \times p_D$ of D_2O in the sample buffer. (Note that for low molar fractions of D_2O, actually HDO is present in the sample buffer which has twice the molar fraction as D_2O. However, the likelihood of an exchange from NH to ND is only half in the presence of HDO compared to D_2O. Both pre-factors cancel out such that the final pseudo first order rate constant is the same. We therefore use the simplified description involving D_2O).

For the rate equation describing the time evolution of the molar fraction of the amide group $[NH]$ we obtain:

$$\frac{d}{dt} [NH] = - k_{HD} [NH] + k_{DH} [ND] \quad (6)$$

Solving the linear differential equation and using the initial condition [NH] (t = 0) = $[NH]_0$ and [ND] (t=0) = 0, as only ^{15}N bound to protons is present after the refocused INEPT and start of the relaxation period, yields:

$$[NH](t) = \left(k_{HD} [NH]_0 e^{-(k_{HD}+k_{DH})t} + k_{DH} [NH]_0\right) / (k_{HD} + k_{DH}) \quad (7a)$$

Using the relations described in equation (5) this yields:

$$[NH](t) = \left(k_{NH} p_D [NH]_0 e^{-k_{NH}(p_D+p_H)t} + k_{NH} p_H [NH]_0\right) / (k_{NH}(p_D + p_H)) . (7b)$$

which further simplifies with $p_D + p_H = 1$ to

$$[NH](t) = \left(p_D e^{-k_{NH} t} + p_H\right)[NH]_0 \quad . (7c)$$

an thus $k_{ex} = k_{NH}$. That means that the chemical shift tensor gets modulated at the amide solvent exchange rate.

The chemical shift difference induced by the deuterium isotope effect is $\Delta\delta(N) = 687 \pm 35$ ppb [46] which amounts to ca. $\Delta\omega = 250$ rad s^{-1} and $\Delta\omega/2\pi = 40$ Hz at a magnetic field strength of 14.1 T (corresponding to a proton Larmor frequency of 600 MHz). With an amide exchange rate constant, k_{ex}, in the range between 10 to 100 s^{-1} at pH 7.4 and 303 K, the exchange process is neither in the fast exchange limit, $\Delta\omega \ll k$, nor in the slow exchange limit, $\Delta\omega \gg k$, but rather on an intermediate timescale. To estimate the exchange contribution on ^{15}N R_2 as a result of solvent exchange in the sample buffer, the following formula was used:

$$R_{ex} \approx \frac{p_a p_b k_{ex}}{1 + \left(\frac{k_{ex}}{\Delta\omega}\right)^2} \qquad (8).$$

as described in [59]. For 4 % D_2O, described by $p_a = 0.96$ and $p_b = 0.04$, eq. (8) yields $R_{ex} = 3.31$ s^{-1} for $k_{ex} = 100$ s^{-1}, $R_{ex} = 0.38$ s^{-1} for $k_{ex} = 10$ s^{-1} and $R_{ex} = 0.04$ s^{-1} for $k_{ex} = 1$ s^{-1} . While for 50 % D_2O $R_{ex} = 21.55$ s^{-1} for $k_{ex} = 100$ s^{-1}, $R_{ex} = 2.5$ s^{-1} for $k_{ex} = 10$ s^{-1} and $R_{ex} = 0.25$ s^{-1} for $k_{ex} = 1$ s^{-1} are estimated. Please note eq. (8) is strictly speaking no longer fulfilled in the latter case because $p_a = p_b = 0.5$ but can be used to get approximate values. Furthermore, effects like a different dipolar coupling interaction for ^{15}N-D vs. ^{15}N-H or the quadrupole moment of the deuteron have not been taken into consideration.

Nonetheless, with this rough estimate, an idea on the order of magnitude of the exchange contribution caused by the deuterium isotope effect modulating the ^{15}N chemical shift tensor as a result of chemical exchange between amide protons and deuterons is obtained. It is in good agreement with the experimentally observed D_2O dependency of the ^{15}N R_2. There is an additional loss mechanism by solvent exchange from a ^{15}N-^1H moiety to ^{15}N-D moiety during the relaxation delay making the latter moiety impossible to detect by ^1H acquisition [60]. This effect sales linear with the D_2O concentration and can explain partly the observed increase in ^{15}N R_2 rate constants for the sample containing 50% D_2O. As deuterium is not decoupled during the relaxation period, also ^{15}N-D anti-phase magnetization will evolve during the relaxation period and contribute by scalar relaxation of the second kind. This effect also scales linear with the D_2O concentration in the sample buffer; further an^{15}N-H spin pair will show a higher ^{15}N R_2 rate constant than a ^{15}N-D spin pair[61,62]. Scalar relaxation of the second kind induced by the exchange of amide protons can also be an additional loss mechanism in Hahn-echo based ^{15}N R_2 measurements[63], however we did not observe any significant differences when changing the RF amplitude of the waltz64 ^1H decoupling scheme from 2.5 kHz to 6 kHz (Fig. S4).

The use of an external deuterium lock for ^{15}N R_2 relaxation measurements

The findings discussed above request ^{15}N relaxation R_2 measurements in absence of D_2O in the sample buffer. This is achieved by using a coaxial insert by Wilmad comprising D_2O inserted into a 5 mm thin-wall NMR tube containing the ^{15}N-labeled α-synuclein in its D_2O-free buffer. The external D_2O reference is added by inserting a 2 mm capillary which leads to a loss of 16% effective sample volume for a 5 mm NMR tube. No line broadening as result of potential B_0 inhomogeneity was observed, however the quality of water suppression was slightly worse and the spectral noise increased slightly.

This approach allows for ^{15}N relaxation measurements using external D_2O as a lock substance. Fig. 4 shows a comparison of the Hahn-echo based ^{15}N R_2, relaxation rate constants of α-synuclein in presence of 4% D_2O and in the absence of any D_2O in the sample buffer, at two temperatures 283 K and 303 K. Interestingly, while rate constants at pH 7.4 and 283 K vary little (Fig. 4a), at 303 K rate constants measured in the absence of D_2O are systematically lower than in the presence of only 4% of D_2O, with

the exception of the last ~30 residues (Fig. 4b). Similar observations have been made with a D_2O-free sample that lacked an external locking substance and was thus measured without locking the magnetic field (data not shown).
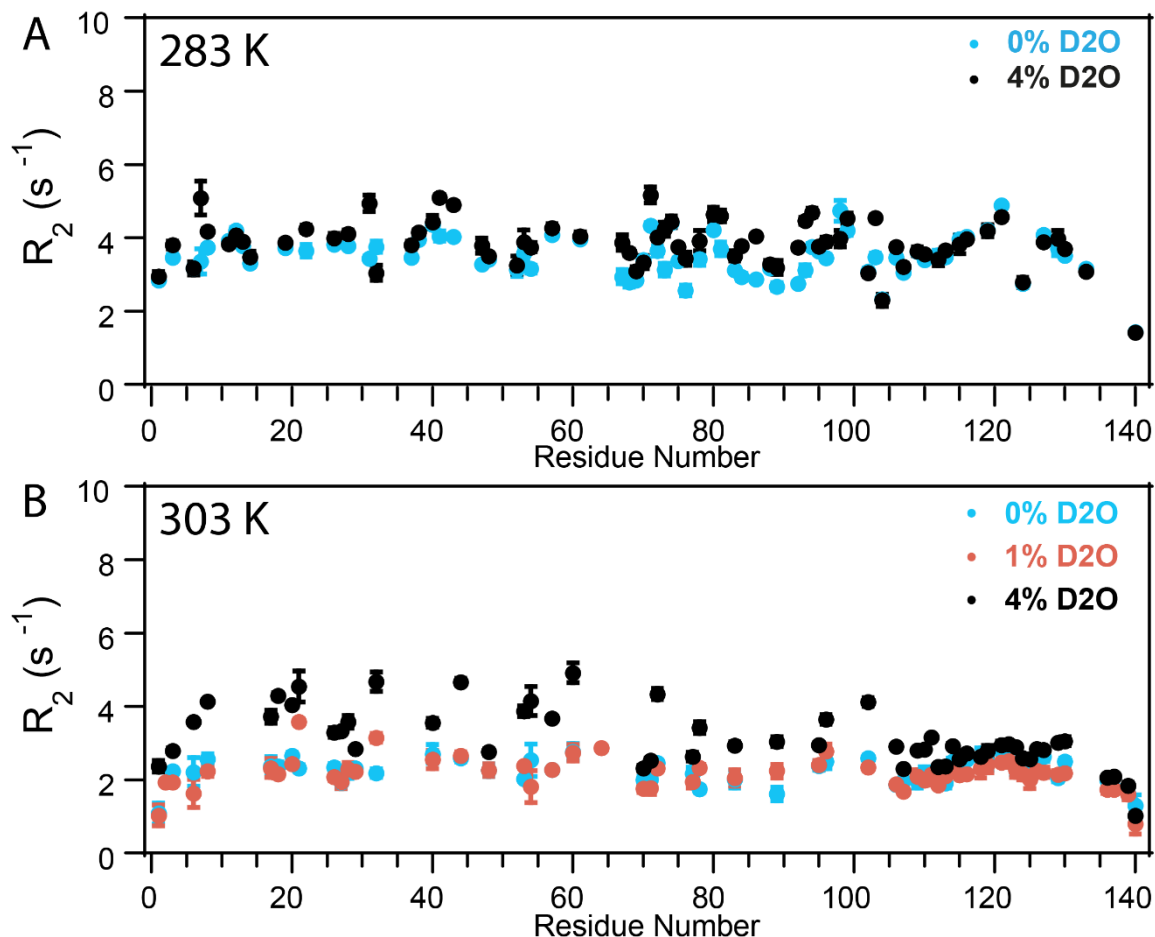

Fig. 4. The importance of using a D₂O molar fraction as low as 1% or an external deuterium lock for the measurement of Hahn-echo based ¹⁵N relaxation rates of ¹⁵N-labeled α-synuclein: ¹⁵N relaxation rates in the absence of D₂O versus a D₂O content of 4% and 1% in the sample buffer. Hahn-echo based ^{15}N R_2 rate constants of α-synuclein measured with the pulse sequence shown in Fig. 1. Rate constants measured in the presence of 4% D_2O (black) are compared to those measured without D_2O (light blue) in the sample buffer at pH 7.4 and temperatures of (A) 283 K and (B) 303 K (using an external deuterium lock). When using a D_2O molar fraction of 1% (red), even at 303 K the effect is small.

The effect of sample internal D_2O on the ^{15}N R_2 relaxation measurements on the folded protein domain PDZ2

To illustrate that the documented deuterium exchange effects are visible not only for IDPs as illustrated above for α-synuclein, relaxation measurements on the ^{15}N-labeled PDZ2 domain of human phosphatase ^{40} were performed at pH 8.0 and a temperature of 303 K. The impact of the presence of D$_2$O in the sample buffer on the measured Hahn-echo based ^{15}N R$_2$ rate constants for the PDZ2 domain is illustrated in Fig. 5. Some residues in loop regions (i.e. Asn16, Gly19, Gly24, Gly25, Gly34, Gly50, and Gly63) show a systematic increase in the ^{15}N R$_2$ rate constants when measured in the presence of only 4% D$_2$O in the sample buffer compared to the sample without any D$_2$O in the sample buffer, using an external D$_2$O reference. Glycine residues appear thereby to be overrepresented which is attributed to their overall fast intrinsic amide-water exchange [64].
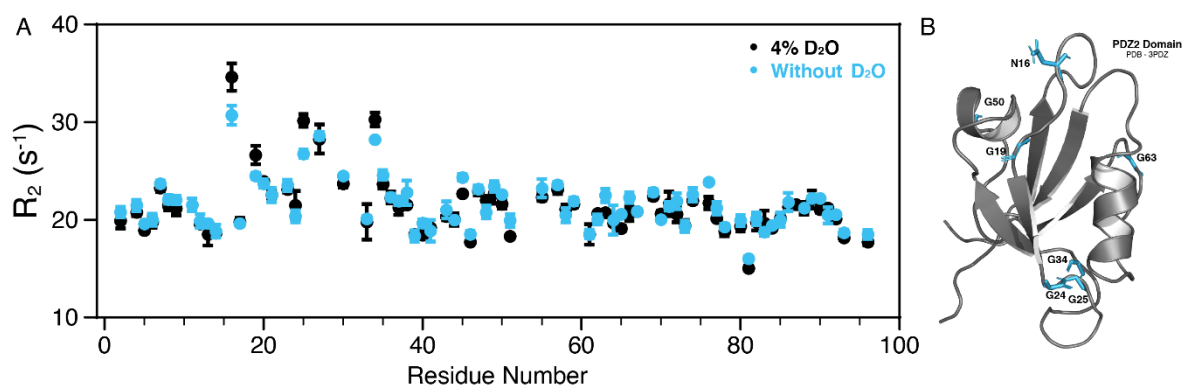

Fig. 5. **Impact of D$_2$O on the Hahn-echo based ^{15}N R$_2$ rate constants of the globular domain PDZ2.** (A) ^{15}N R$_2$ relaxation rates using the pulse sequence of Fig. 1 were measured on the PDZ2 domain of human phosphatase ^{40} in the presence of 4% D$_2$O (black) and absence of D$_2$O (blue) in the buffer. In the latter case, a sample-external D$_2$O inside an insert was used for locking the magnetic field. The influence of D$_2$O is pronounced for a few residues in loops (i.e. Asn16, Gly19, Gly24, Gly25, Gly34, Gly50, and Gly63) with a strong overrepresentation of glycine residues attributed to their overall fast intrinsic amide-water exchange. (B) The residues for which the relaxation was altered by the absence of D$_2$O are highlighted in blue on the structure of PDZ2 domain (PDB ID: 3PDZ) shown in a ribbon representation.

The impact of internal D$_2$O on CPMG-based relaxation dispersion experiments

Because of the significant R$_{ex}$ contribution on the measured Hahn-echo based ^{15}N R$_2$ rate constant caused by D$_2$O in the sample buffer, we simulated the anticipated R$_{ex}$ contributions in a CPMG relaxation dispersion experiment. At pH 7.4 and 25˚C (298 K), for solvent-exposed residues the amide exchange rate will assume values in the order of k$_{NH}$ = 10 s^{-1} to k$_{NH}$ = 100 s^{-1},[49] depending on the extend of solvent exposure of the respective residue. Calculations for different amounts of D$_2$O in the sample buffer (1%, 4% and 10%) are shown in Fig. 6. As illustrated in Fig. 6A, in the presence of 10% D$_2$O for a residue

showing fast amide exchange with = 100 s^{-1} the R_{ex} contribution due to D_2O in the sample buffer is present at CPMG frequencies less than 100 s^{-1}, but is significantly reduced for CPMG frequencies ν_{cpmg} > 100 s^{-1}, and fully averaged out for a CPMG frequency ν_{cpmg} = 500 s^{-1}. The observed effects scales approximately linearly with the amount of D_2O in the sample buffer (Fig. 6A). However, even for a D_2O molar fraction as low as 1%, the maximum R_{ex} contribution goes up to 1 s^{-1} (at low CPMG frequencies with ν_{cpmg} < 100 s^{-1}). While this may be negligible for the structured part of a large globular protein with an R_2 rate constants of e.g. 50 s^{-1}, it amounts to an error of 50% for an IDP with a rate constant of e.g. 2 s^{-1}. For an amide exchange rate constant of k_{NH} < 10 s^{-1}, the effect is reduced by approximately ten-fold and therefore less critical for only low amounts of D_2O in the sample buffer (Fig. 6B). Overall, the R_{ex} contribution roughly scales linearly with the percentage of D_2O in the sample buffer and the given amide exchange rate constant k_{NH}. Therefore, at lower pH < 6.5 and temperatures around or below room temperature, where the amide exchange rate will usually be less than k_{NH} < 10 s^{-1}, at 1% of D_2O in the sample buffer the R_{ex} contribution by D_2O can be safely ignored. When approaching physiological pH and temperature however, the amide exchange rate constants for many residues can approach values of 100 s^{-1} [49]. Then, for ν_{cpmg} < 100 s^{-1} the R_{ex} contribution by D_2O in the sample buffer can add a significant systematic error on measured R_2 relaxation dispersion profiles of IDPs that have low $R_{2,0}$ auto-relaxation constants.
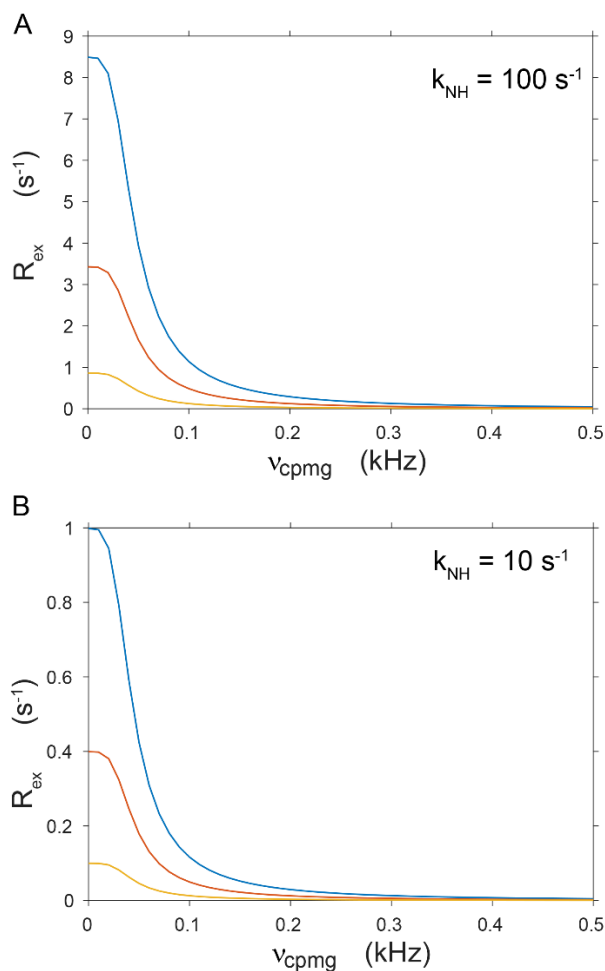
Fig. 6. Simulated CPMG relaxation dispersion curves in presence of different amounts of D$_2$O in the sample buffer. The R$_{ex}$ contribution to ^{15}N R$_2$ is shown as a function of the applied CPMG frequency, with v_cpmg = 1 / (2 τ_cp) and τ_cpmg/2 – 180˚ (N) – τ_cpmg/2 constituting the basic CPMG block. Data are shown for an amide exchange rate constant of (A) k$_{NH}$ = 100 s^{-1} and 10 % (blue), 4% (red) and 1% (yellow) D$_2$O in the sample buffer as well as for amide exchange rate constant of (B) k$_{NH}$ = 10 s^{-1} and 10 % (blue), 4% (red) and 1% (yellow) D$_2$O in the sample buffer. See Materials and Methods for further details.

We have tested the impact of D$_2$O in sample buffer on the extracted CPMG-based ^{15}N R$_2$ rate constants experimentally with α-synuclein. Indeed, at a CPMG frequency of 100 Hz, the exchange contribution induced by D$_2$O appears to be reduced substantially. However, at a low CPMG frequency of 20 Hz we observe substantial R$_{ex}$ contributions, leading to increased ^{15}N R$_2$ rate constants in the presence of 10% D$_2$O (Fig. 7).

Finally, we measured also standard ^{15}N $R_{1\rho}$ relaxation measurements[42] with a spin-lock RF amplitude of 2 kHz on α-synuclein (pH 7.4, 303 K). As expected, when comparing ^{15}N $R_{1\rho}$ rate constants in the presence of 10% D_2O and absence of D_2O in the sample buffer, we observe only little differences, which is attributed to the loss of measurable magnetization from the exchange to a N-D moiety during the relaxation delays (Fig. 8).

Therefore, the R_{ex} contribution induced by D_2O in the sample buffer appears to be suppressed for a standard ^{15}N $R_{1\rho}$ experiment employing a spin-lock RF amplitude of 2 kHz.
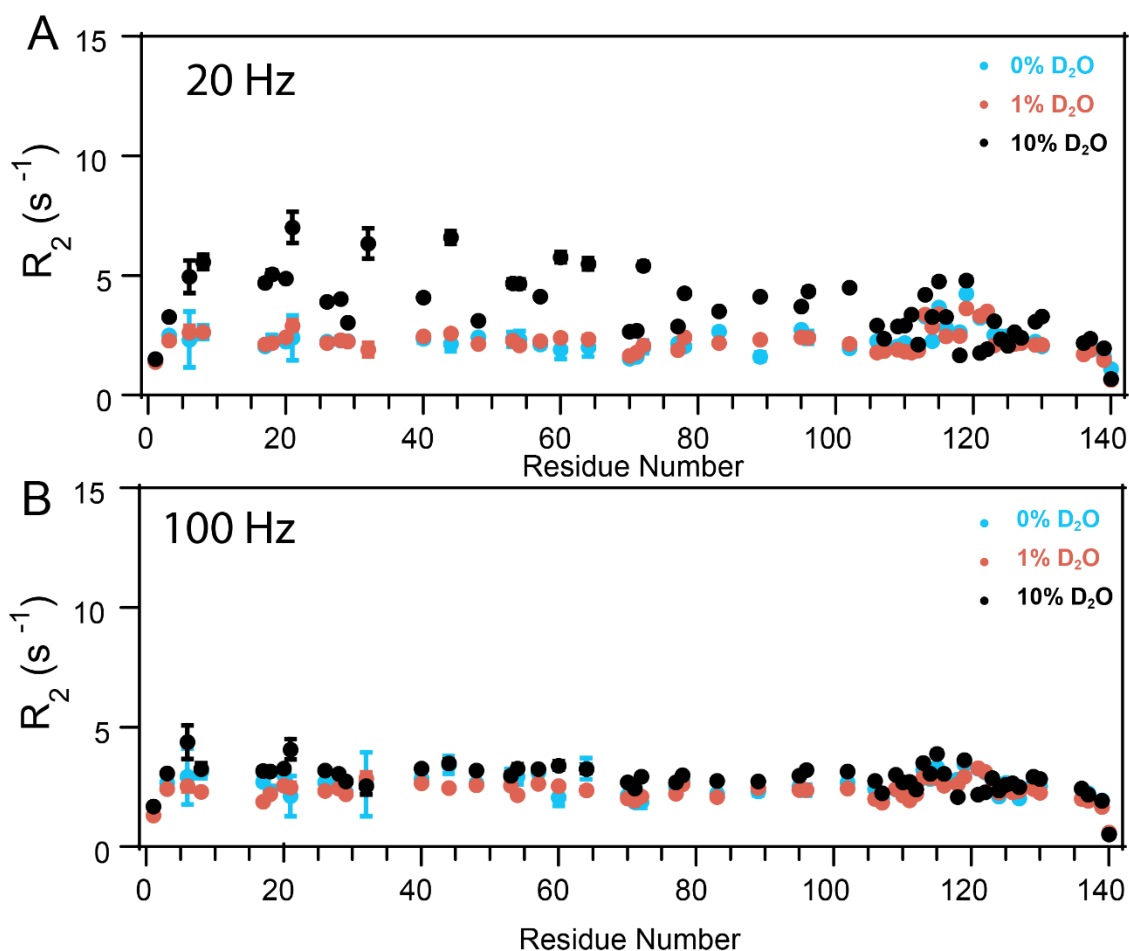

Fig. 7. Impact of D_2O on CPMG-based ^{15}N R_2 rate constants of α-synuclein with weak CPMG frequencies (i.e. 20 Hz and 100 Hz). CPMG-based ^{15}N R_2 rate constants of α-synuclein were measured at pH 7.4 and at 303 K in the presence of 10% D_2O (black), 1% D_2O (red) and in the absence of D_2O in the sample buffer (light blue). The CPMG frequency was (A) 20 Hz and (B) 100 Hz.
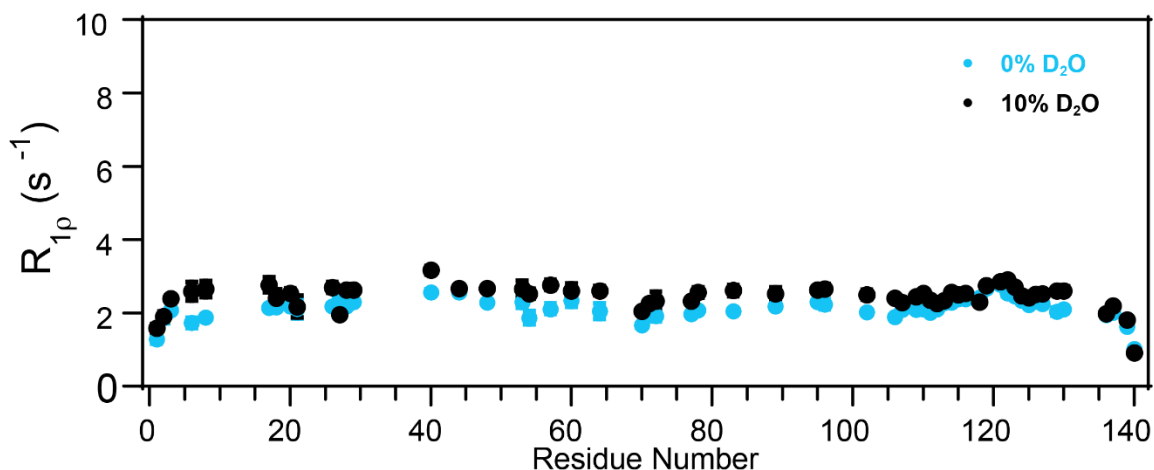
Fig. 8. Little impact of D₂O on ¹⁵N $R_{1\rho}$ rate constants of α-synuclein under a spin-lock frequency (i.e. 2 kHz). ¹⁵N $R_{1\rho}$ rate constants for α-synuclein (pH 7.4, 303 K) were measured using a spin-lock RF amplitude of 2 kHz in absence (blue) and presence (black) of 10% D₂O.

Discussion

The presented data shows that at near physiological pH (i.e. pH 7.4) and physiological temperatures of 30-37 ˚C, solvent exchange of the amide protons with deuterium in the sample buffer can impact Hahn-echo based ¹⁵N R_2 measurements significantly due to the deuterium isotope effect even at low molar fraction of D₂O in the sample buffer (as low as 4%). This effect is pronounced for several loop residues in the folded protein domain PDZ2 but is most prominent in the intrinsically disordered protein α-synuclein. As many IDPs show very low ¹⁵N R_2 rate constants (< 5 s⁻¹) due to their high intrinsic flexibility, even a small systematic artifactual R_{ex} contribution of e.g. 1 s⁻¹ can lead to a large error in the data. Therefore, for Hahn-echo based ¹⁵N R_2 measurements the use of only a very low D₂O molar fraction in the sample buffer, as low as 1%, is necessary or, alternatively, the use of an external D₂O lock using a coaxial capillary insert.

Since IDPs form a large part of the human proteome (30-40%) and play an essential role in cellular signaling and regulation of many biomolecular interactions [65-67] , over the last two decades solution-state NMR provided important insights to characterize secondary structure propensity, conformational space [68,69] and non-local and local dynamics of IDPs using mainly ¹⁵N CPMG based relaxation dispersion experiments [15-18,67,69-80]. Several experimental strategies have been designed to allow the recording of

[1]H-^{15}N correlation spectra [81,82] and CPMG relaxation experiments of IDPs under physiological conditions and obviate the influence of amide exchange [43,83], but the adverse impact of D_2O through the isotope effect has to our knowledge escaped attention. At physiological pH and near physiological temperatures, we observed a substantial R_{ex} contribution induced by D_2O in the sample buffer that is not suppressed for a low CPMG frequency of 20 kHz. That finding is in agreement with simulated data that predict a substantial contribution for CPMG frequencies < 100 Hz. At a CPMG frequency of 100 Hz the R_{ex} contribution induced by D_2O in the sample buffer appears however suppressed, in agreement between experimental and simulated data.

For standard [15]N R_2 measurements (aiming at the investigation of ps-ns dynamics), employing a CPMG frequency of at least 100 Hz as well as proton decoupling [83] [43] (to counteract the adverse effect of amide exchange), the effect is however reduced substantially and will not lead to an artificial increase of the [15]N R_2 rate constants. Also, in standard [15]N $R_{1\rho}$ experiments that spin-lock ^{15}N transverse magnetization, deuterium isotope effects will be suppressed, as long as the spin-lock RF amplitude, given in frequency units, is significantly faster than the amide exchange rate constants – which is usually the case, e.g. for an RF amplitude of 2 kHz and an amide exchange rate in the order of 100 s^{-1}.

Therefore, the discussed effect is uncritical for standard [15]N R_2 experiments that aim at characterizing ns-ps dynamics and therefore suppress R_{ex} contributions by spin-lock fields with high RF amplitude in the case of $R_{1\rho}$ measurements or high CPMG frequencies in the case of ^{15}N CPMG-based [15]N R_2 experiments. But it is important for standard [15]N R_2 experiments that aim at the quantification of R_{ex} contributions due to conformational dynamics on a μs-ms timescale, such as Hahn-echo based [15]N R_2 experiments or the more popular CPMG-based [15]N R_2 relaxation dispersion experiments. (For both experiments it is important to employ proton decoupling during the relaxation period such as suggested by [83] and [43] to counteract adverse effects of amide exchange.) The deuterium induced R_{ex} contribution is less critical for globular proteins with higher [15]N R_2 rate constants and in the presence of large R_{ex} effects due to conformational dynamics, in the order of e.g. 10 s^{-1}. But it can become very critical for the interpretation of CPMG-based relaxation dispersion curves or Hahn-echo based [15]N R_2 experiments of intrinsically disordered proteins (IDPs) that are characterized by low [15]N R_2 rate constants (in the

order of a few s^{-1}) and where even a small R$_{ex}$ contribution in the order of e.g. 0.5 s^{-1} or more can add to the ^{15}N R$_2$ rate constant substantially.

Indeed, for CPMG-based relaxation dispersion experiments the CPMG frequency for the first, low frequency data points, can be lower than the solvent-exchange rate, depending on the settings for the minimal frequency of the CPMG block in relaxation dispersion experiments, and thus exchange with deuterons in the sample buffer may adversely affect the accuracy of the extracted results and may lead to artificial R$_{ex}$ effects, which originate from deuterium exchange and a modulation of the ^{15}N chemical shift tensor through the deuterium isotope effect rather than conformational dynamics. For Hahn-echo based ^{15}N R$_2$ measurements, that do not suppress but detect all R$_{ex}$ contributions, R$_{ex}$ contributions caused by the deuterium isotope effect are never suppressed and therefore most severe. For high precision CPMG-based relaxation measurements as well as Hahn-echo based ^{15}N R$_2$ experiments that aim at the quantification of μs-ms dynamics, we therefore recommend also the use of a very low D$_2$O content, as low as 1%, or, alternatively, the use of an external deuterium reference, which is easily possible using commercially available NMR tube inserts. This is most critical for IDPs or very flexible loop region in globular proteins that are characterized by low ^{15}N R$_2$ rate constants.

Conclusion

The determination of the ^{15}N R$_2$ relaxation rate constants is a standard NMR experiment in the evaluation of the dynamics of proteins, including both folded and intrinsically disordered protein entities. While measurements at low pH (< 6.5) or low temperatures (< 10 ˚C) are usually uncritical because of low solvent amide exchange rates, at physiological pH and temperatures, effects related to solvent amide exchange can lead to artifactual R$_{ex}$ contributions.

The presented results show that the presence of D$_2$O > 1% in the sample buffer can deteriorate the accuracy of the rates constants measured using a Hahn-echo based ^{15}N R$_2$ experiments and also for low CPMG-frequency data points (< 100 Hz) in CPMG relaxation dispersion experiments. For CMPG frequencies > 100 Hz as well as for ^{15}N R$_{1\rho}$ experiments that apply a high-power spin-lock RF amplitude, of e.g. 2 kHz, the modulation of the ^{15}N chemical shift tensor by deuterium isotope effect due to amide

exchange between N-H and N-D is suppressed and will not lead to artificial R_{ex} contributions, even in the presence of larger amounts of D_2O in the sample buffer. Therefore, the discussed effect is uncritical for standard ^{15}N R_2 experiments that aim at the characterization of ps-ns dynamics. For Hahn-echo based ^{15}N R_2 measurement or CPMG-based ^{15}N R_2 relaxation dispersion experiments at near physiological conditions that aim at the characterization of μs-ms dynamics, we however recommend the use of a very low D_2O content in the sample buffer, as low as 1% molar fraction or, alternatively, the use of an external deuterium reference. This applies both to in vitro or in-cell NMR experiments [84-89] and is most important for intrinsically disordered proteins that are characterized by low ^{15}N R_2 rate constants and where even small R_{ex} contributions can lead to large changes in the measured ^{15}N R_2 rate constant.

References

1. Mittermaier, A.K. & Kay, L.E. Observing biological dynamics at atomic resolution using NMR. *Trends Biochem Sci.* **34**, 601-611 (2009).
2. Palmer, A.G. Enzyme Dynamics from NMR Spectroscopy. *Acc. Chem. Res.* **48**, 457-465 (2015).
3. Salvi, N., Ulzega, S., Ferrage, F. & Bodenhausen, G. Time Scales of Slow Motions in Ubiquitin Explored by Heteronuclear Double Resonance. *J. Am. Chem. Soc.* **134**, 2481-2484 (2012).
4. Pelupessy, P., Ravindranathan, S. & Bodenhausen, G. Correlated motions of successive amide N-H bonds in proteins. . *J. Biomol. NMR* **25**, 265-280 (2003).
5. Fenwick, R.B. et al. Weak Long-Range Correlated Motions in a Surface Patch of Ubiquitin Involved in Molecular Recognition. *J. Am. Chem. Soc.* **133**, 10336-10339 (2011).
6. Vogeli, B. et al. Towards a true protein movie: A perspective on the potential impact of the ensemble-based structure determination using exact NOEs. *J. Magn. Reson.* **241**, 53-59 (2014).
7. Vogeli, B. & Yao, L.S. Correlated Dynamics between Protein HN and HC Bonds Observed by NMR Cross Relaxation. *J. Am. Chem. Soc.* **131**, 3668-3678 (2009).
8. Mittermaier, A. & Kay, L.E. Review - New tools provide new insights in NMR studies of protein dynamics. *Science* **312**, 224-228 (2006).
9. Vallurupalli, P., Bouvignies, G. & Kay, L.E. Studying "Invisible" Excited Protein States in Slow Exchange with a Major State Conformation. *J. Am. Chem. Soc.* **134**, 8148-8161 (2012).
10. Palmer, A.G. NMR characterization of the dynamics of biomacromolecules. *Chem. Rev.* **104**, 3623-3640 (2004).
11. Lange, O.F. et al. Recognition dynamics up to microseconds revealed from an RDC-derived ubiquitin ensemble in solution. *Science* **320**, 1471-1475 (2008).
12. Fawzi, N.L., Ying, J.F., Ghirlando, R., Torchia, D.A. & Clore, G.M. Atomic-resolution dynamics on the surface of amyloid-beta protofibrils probed by solution NMR. *Nature* **480**, 268-U161 (2011).
13. Charlier, C., Cousin, S.F. & Ferrage, F. Protein dynamics from nuclear magnetic relaxation. *Chem. Soc. Rev.* **45**, 2410-2422 (2016).
14. Charlier, C. et al. Nanosecond Time Scale Motions in Proteins Revealed by High-Resolution NMR Relaxometry. *J. Am. Chem. Soc.* **135**, 18665-18672 (2013).

15. Kay, L.E., Torchia, D.A. & Bax, A. Backbone Dynamics of Proteins as Studied by N-15 Inverse Detected Heteronuclear Nmr-Spectroscopy - Application to Staphylococcal Nuclease. *Biochemistry* **28**, 8972-8979 (1989).

16. Farrow, N.A. et al. Backbone Dynamics of a Free and a Phosphopeptide-Complexed Src Homology-2 Domain Studied by N-15 Nmr Relaxation. *Biochemistry* **33**, 5984-6003 (1994).

17. Loria, J.P., Rance, M. & Palmer, A.G. A relaxation-compensated Carr-Purcell-Meiboom-Gill sequence for characterizing chemical exchange by NMR spectroscopy. *J. Am. Chem. Soc.* **121**, 2331-2332 (1999).

18. Mulder, F.A.A., Skrynnikov, N.R., Hon, B., Dahlquist, F.W. & Kay, L.E. Measurement of slow (mu s-ms) time scale dynamics in protein side chains by N-15 relaxation dispersion NMR spectroscopy: Application to Asn and Gln residues in a cavity mutant of T4 lysozyme. *J. Am. Chem. Soc.* **123**, 967-975 (2001).

19. Kiteyski-LeBlanc, J.L. et al. Investigating the Dynamics of Destabilized Nucleosomes Using Methyl-TROSY NMR. *J. Am. Chem. Soc.* **140**, 4774-4777 (2018).

20. Tugarinov, V. & Kay, L.E. Methyl groups as probes of structure and dynamics in NMR studies of high-molecular-weight proteins. *Chembiochem* **6**, 1567-77 (2005).

21. Tolman, J.R., Al-Hashimi, H.M., Kay, L.E. & Prestegard, J.H. Structural and dynamic analysis of residual dipolar coupling data for proteins. *J. Am. Chem. Soc.* **123**, 1416-1424 (2001).

22. Peti, W., Meiler, J., Bruschweiler, R. & Griesinger, C. Model-free analysis of protein backbone motion from residual dipolar couplings. *J. Am. Chem. Soc.* **124**, 5822-5833 (2002).

23. Vogeli, B. Cross-correlated relaxation rates between protein backbone H-X dipolar interactions. *J. Biomol. NMR* **67**, 211-232 (2017).

24. Pintacuda, G. & Otting, G. Identification of protein surfaces by NMR measurements with a paramagnetic Gd(III) chelate. *J. Am. Chem. Soc.* **124**, 372-373 (2002).

25. Iwahara, J. & Clore, G.M. Detecting transient intermediates in macromolecular binding by paramagnetic NMR. *Nature* **440**, 1227-1230 (2006).

26. Xu, X.F. et al. Dynamics in a pure encounter complex of two proteins studied by solution scattering and paramagnetic NMR spectroscopy. *J. Am. Chem. Soc.* **130**, 6395-6403 (2008).

27. Vogeli, B., Kazemi, S., Guntert, P. & Riek, R. Spatial elucidation of motion in proteins by ensemble-based structure calculation using exact NOEs. *Nat. Struct. Mol. Biol.* **19**, 1053-U110 (2012).

28. Showalter, S.A. & Bruschweiler, R. Validation of molecular dynamics simulations of biomolecules using NMR spin relaxation as benchmarks: Application to the AMBER99SB force field. *J. Chem. Theory Comput.* **3**, 961-975 (2007).

29. Markwick, P.R.L., Showalter, S.A., Bouvignies, G., Bruschweiler, R. & Blackledge, M. Structural dynamics of protein backbone phi angles: extended molecular dynamics simulations versus experimental (3) J scalar couplings. *J. Biomol. NMR* **45**, 17-21 (2009).

30. Bouvignies, G. et al. Identification of slow correlated motions in proteins using residual dipolar and hydrogen-bond scalar couplings. *Proc. Natl. Acad. Sci.* U S A **102**, 13885-13890 (2005).

31. Lindorff-Larsen, K., Best, R.B., DePristo, M.A., Dobson, C.M. & Vendruscolo, M. Simultaneous determination of protein structure and dynamics. *Nature* **433**, 128-132 (2005).

32. Camilloni, C. & Vendruscolo, M. NMR chemical shifts and protein dynamics. *FEBS J.* **279**, 529-529 (2012).

33. Kannan, A., Camilloni, C., Sahakyan, A.B., Cavalli, A. & Vendruscolo, M. A Conformational Ensemble Derived Using NMR Methyl Chemical Shifts Reveals a Mechanical Clamping Transition That Gates the Binding of the HU Protein to DNA. *J. Am. Chem. Soc.* **136**, 2204-2207 (2014).

34. Case, D.A. Chemical shifts in biomolecules. *Curr. Opin. Struct. Biol.* **23**, 172-176 (2013).

35. Luginbuhl, P. & Wuthrich, K. Semi-classical nuclear spin relaxation theory revisited for use with biological macromolecules. *Prog. Nucl. Magn. Reson. Spectrosc.* **40**, 199-247 (2002).

36. Cavanagh, J., Fairbrother, W.J., Palmer, A.G., Rance, M. & Skelton, N.J. Protein NMR Spectroscopy. *Academic Press* (2007).

37. Johnson, M., Coulton, A.T., Geeves, M.A. & Mulvihill, D.P. Targeted amino-terminal acetylation of recombinant proteins in E. coli. *PLoS One* **5**, e15801 (2010).

38. Huang, C., Ren, G., Zhou, H. & Wang, C.C. A new method for purification of recombinant human alpha-synuclein in Escherichia coli. *Protein Expr. Purif.* **42**, 173-7 (2005).

39. Campioni, S. et al. The presence of an air-water interface affects formation and elongation of alpha-Synuclein fibrils. *J. Am. Chem. Soc.* **136**, 2866-75 (2014).

40. Gianni, S. et al. The kinetics of PDZ domain-ligand interactions and implications for the binding mechanism. *J. Biol. Chem.* **280**, 34805-12 (2005).

41. Lakomek, N.A. et al. Internal Dynamics of the Homotrimeric HIV-1 Viral Coat Protein gp41 on Multiple Time Scales. *Angew. Chem. Int. Ed. Engl.* **52**, 3911-3915 (2013).

42. Lakomek, N.A., Ying, J.F. & Bax, A. Measurement of N-15 relaxation rates in perdeuterated proteins by TROSY-based methods. *J. Biomol. NMR* **53**, 209-221 (2012).

43. Yuwen, T. & Skrynnikov, N.R. Proton-decoupled CPMG: A better experiment for measuring N-15 R-2 relaxation in disordered proteins. *J. Magn. Reson.* **241**, 155-169 (2014).

44. Palmer, A.G., Kroenke, C.D. & Loria, J.P. Nuclear magnetic resonance methods for quantifying microsecond-to-millisecond motions in biological macromolecules. *Nuclear Magnetic Resonance of Biological Macromolecules, Pt B* **339**, 204-238 (2001).

45. Ishima, R. & Torchia, D.A. Estimating the time scale of chemical exchange of proteins from measurements of transverse relaxation rates in solution. *J. Biomol. NMR* **14**, 369-372 (1999).

46. Tugarinov, V. Indirect use of deuterium in solution NMR studies of protein structure and hydrogen bonding. *Prog. Nucl. Magn. Reson. Spectrosc.* **77**, 49-68 (2014).

47. Wagner, G. & Wuthrich, K. Structural Interpretation of the Amide Proton-Exchange in the Basic Pancreatic Trypsin-Inhibitor and Related Proteins. *J. Mol. Biol.* **134**, 75-94 (1979).

48. Dempsey, C.E. Hydrogen exchange in peptides and proteins using NMR-spectroscopy. *Prog. Nucl. Magn. Reson. Spectrosc.* **39**, 135-170 (2001).

49. Croke, R.L., Sallum, C.O., Watson, E., Watt, E.D. & Alexandrescu, A.T. Hydrogen exchange of monomeric alpha-synuclein shows unfolded structure persists at physiological temperature and is independent of molecular crowding in Escherichia coli. *Prot. Sci.* **17**, 1434-1445 (2008).

50. Wang, C., Rance, M. & Palmer, A.G., 3rd. Mapping chemical exchange in proteins with MW > 50 kD. *J. Am. Chem. Soc.* **125**, 8968-9 (2003).

51. Skrynnikov, N.R. & Ernst, R.R. Detection of intermolecular chemical exchange through decorrelation of two-spin order. *J. Magn. Reson.* **137**, 276-280 (1999).

52. Pervushin, K., Riek, R., Wider, G. & Wuthrich, K. Attenuated T-2 relaxation by mutual cancellation of dipole-dipole coupling and chemical shift anisotropy indicates an avenue to NMR structures of very large biological macromolecules in solution. *Proc. Natl. Acad. Sci.* U S A **94**, 12366-12371 (1997).

53. Favier, A. & Brutscher, B. Recovering lost magnetization: polarization enhancement in biomolecular NMR. *J. Biomol. NMR* **49**, 9-15 (2011).

54. Pervushin, K.V., Wider, G. & Wuthrich, K. Single transition-to-single transition polarization transfer (ST2-PT) in [N-15,H-1]-TROSY. *J. Biomol. NMR* **12**, 345-348 (1998).

55. Kay, L.E., Keifer, P. & Saarinen, T. Pure Absorption Gradient Enhanced Heteronuclear Single Quantum Correlation Spectroscopy with Improved Sensitivity. *J. Am. Chem. Soc.* **114**, 10663-10665 (1992).

56. Khare, D., Alexander, P. & Orban, J. Hydrogen bonding and equilibrium protium-deuterium fractionation factors in the immunoglobulin G binding domain of protein G. *Biochemistry* **38**, 3918-3925 (1999).

57. Henry, G.D., Weiner, J.H. & Sykes, B.D. Backbone Dynamics of a Model Membrane-Protein - Measurement of Individual Amide Hydrogen-Exchange Rates in Detergent-Solubilized M13 Coat Protein Using C-13 Nmr Hydrogen-Deuterium Isotope Shifts. *Biochemistry* **26**, 3626-3634 (1987).

58. Connelly, G.P., Bai, Y.W., Jeng, M.F. & Englander, S.W. Isotope Effects in Peptide Group Hydrogen-Exchange. *Protein Struct Funct Genet* **17**, 87-92 (1993).

59. Millet, O., Loria, J.P., Kroenke, C.D., Pons, M. & Palmer, A.G. The static magnetic field dependence of chemical exchange linebroadening defines the NMR chemical shift time scale. *J. Am. Chem. Soc.* **122**, 2867-2877 (2000).

60. Kim, S., Wu, K.P. & Baum, J. Fast hydrogen exchange affects N-15 relaxation measurements in intrinsically disordered proteins. *J. Biomol. NMR* **55**, 249-256 (2013).

61. Vasos, P.R., Hall, J.B., Kummerle, R. & Fushman, D. Measurement of N-15 relaxation in deuterated amide groups in proteins using direct nitrogen detection. *J. Biomol. NMR* **36**, 27-36 (2006).

62. Xu, J., Millet, O., Kay, L.E. & Skrynnikov, N.R. New spin probe of protein dynamics: Nitrogen relaxation in N-15-H-2 amide groups. . *J. Am. Chem. Soc.* **127**, 3220-3229 (2005).

63. Kateb, F., Pelupessy, P. & Bodenhausen, G. Measuring fast hydrogen exchange rates by NMR spectroscopy. *J. Magn. Reson.* **184**, 108-113 (2007).

64. Bai, Y.W., Milne, J.S., Mayne, L. & Englander, S.W. Primary Structure Effects on Peptide Group Hydrogen-Exchange. *Protein Struct Funct Genet* **17**, 75-86 (1993).

65. Tompa, P. Intrinsically unstructured proteins. *Trends Biochem. Sci.* **27**, 527-533 (2002).

66. Wright, P.E. & Dyson, H.J. Intrinsically unstructured proteins: re-assessing the protein structure-function paradigm. *J. Mol. Biol.* **293**, 321-331 (1999).

67. Wright, P.E. & Dyson, H.J. Intrinsically disordered proteins in cellular signalling and regulation. *Nat. Rev. Mol. Cell. Biol.* **16**, 18-29 (2015).

68. Abyzov, A. et al. Identification of Dynamic Modes in an Intrinsically Disordered Protein Using Temperature-Dependent NMR Relaxation. *J. Am. Chem. Soc.* **138**, 6240-6251 (2016).

69. Salvi, N., Abyzov, A. & Blackledge, M. Atomic resolution conformational dynamics of intrinsically disordered proteins from NMR spin relaxation. *Prog. Nucl. Magn. Reson. Spectrosc* **102**, 43-60 (2017).

70. Sugase, K., Dyson, H.J. & Wright, P.E. Mechanism of coupled folding and binding of an intrinsically disordered protein. *Nature* **447**, 1021-5 (2007).

71. Rezaei-Ghaleh, N., Blackledge, M. & Zweckstetter, M. Intrinsically Disordered Proteins: From Sequence and Conformational Properties toward Drug Discovery. *Chembiochem* **13**, 930-950 (2012).

72. Maltsev, A.S., Chen, J., Levine, R.L. & Bax, A. Site-Specific Interaction between alpha-Synuclein and Membranes Probed by NMR-Observed Methionine Oxidation Rates. *J. Am. Chem. Soc.* **135**, 2943-2946 (2013).

73. Bah, A. et al. Folding of an intrinsically disordered protein by phosphorylation as a regulatory switch. *Nature* **519**, 106-U240 (2015).

74. Zweckstetter, M. Intrinsically Disordered Proteins in Neurodegeneration Markus Zweckstetter. *Biophys. J.* **110**, 2a-2a (2016).

75. Delaforge, E. et al. Deciphering the Dynamic Interaction Profile of an Intrinsically Disordered Protein by NMR Exchange Spectroscopy. *J. Am. Chem. Soc.* **140**, 1148-1158 (2018).

76. Kurzbach, D., Kontaxis, G., Coudevylle, N. & Konrat, R. NMR Spectroscopic Studies of the Conformational Ensembles of Intrinsically Disordered Proteins. *Intrinsically Disordered Proteins Studied by Nmr Spectroscopy* **870**, 149-185 (2015).

77. Lakomek, N.A., Draycheva, A., Bornemann, T. & Wintermeyer, W. Electrostatics and Intrinsic Disorder Drive Translocon Binding of the SRP Receptor FtsY. *Angew. Chem. Int. Ed. Engl.* **55**, 9544-9547 (2016).

78. Schneider, R. et al. Visualizing the Molecular Recognition Trajectory of an Intrinsically Disordered Protein Using Multinuclear Relaxation Dispersion NMR *J. Am. Chem. Soc.* **137**, 1220-1229 (2015).

79. Arai, M., Sugase, K., Dyson, H.J. & Wright, P.E. Conformational propensities of intrinsically disordered proteins influence the mechanism of binding and folding. *Proc. Natl. Acad. Sci.* U S A **112**, 9614-9619 (2015).

80. Charlier, C. et al. Structure and Dynamics of an Intrinsically Disordered Protein Region That Partially Folds upon Binding by Chemical-Exchange NMR. *J. Am. Chem. Soc.* **139**, 12219-12227 (2017).

81. Lopez, J., Schneider, R., Cantrelle, F.X., Huvent, I. & Lippens, G. Studying Intrinsically Disordered Proteins under True In Vivo Conditions by Combined Cross-Polarization and Carbonyl-Detection NMR Spectroscopy. *Angew. Chem. Int. Ed. Engl.* **55**, 7418-7422 (2016).

82. Yuwen, T. & Skrynnikov, N.R. CP-HISQC: a better version of HSQC experiment for intrinsically disordered proteins under physiological conditions. *J. Biomol. NMR* **58**, 175-192 (2014).

83. Kim, S., Wu, K.P. & Baum, J. Fast hydrogen exchange affects ^{15}N relaxation measurements in intrinsically disordered proteins. *J. Biomol. NMR* **55**, 249-56 (2013).

84. Hansel, R., Luh, L.M., Corbeski, I., Trantirek, L. & Dotsch, V. In-Cell NMR and EPR Spectroscopy of Biomacromolecules. *Angew. Chem. Int. Ed. Engl.* **53**, 10300-10314 (2014).

85.   Reckel, S., Hansel, R., Lohr, F. & Dotsch, V. In-cell NMR spectroscopy. *Prog. Nucl. Magn. Reson. Spectrosc* **51**, 91-101 (2007).

86.   Luchinat, E. et al. In-cell NMR reveals potential precursor of toxic species from SOD1 fALS mutants. *Nat. Commun* **5**(2014).

87.   Plitzko, J.M., Schuler, B. & Selenko, P. Structural Biology outside the box - inside the cell. *Curr. Opin. Struct. Biol.* **46**, 110-121 (2017).

88.   Lippens, G. et al. In-cell NMR: from metabolites to macromolecules. *Analyst* **143**, 620-629 (2018).

89.   Theillet, F.X. et al. Structural disorder of monomeric alpha-synuclein persists in mammalian cells. *Nature* **530**, 45-50 (2016).